

This is a repository copy of *Mobile monitoring reveals congestion penalty for vehicle emissions in London*.

White Rose Research Online URL for this paper:

<https://eprints.whiterose.ac.uk/209759/>

Version: Published Version

---

**Article:**

Wilde, Shona E., Padilla, Lauren E., Farren, Naomi J. [orcid.org/0000-0002-5668-1648](https://orcid.org/0000-0002-5668-1648) et al. (7 more authors) (2024) Mobile monitoring reveals congestion penalty for vehicle emissions in London. *Atmospheric Environment*: X. 100241. ISSN 2590-1621

<https://doi.org/10.1016/j.aeaoa.2024.100241>

---

**Reuse**

This article is distributed under the terms of the Creative Commons Attribution (CC BY) licence. This licence allows you to distribute, remix, tweak, and build upon the work, even commercially, as long as you credit the authors for the original work. More information and the full terms of the licence here:

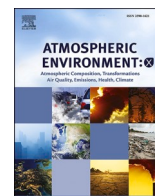
<https://creativecommons.org/licenses/>

**Takedown**

If you consider content in White Rose Research Online to be in breach of UK law, please notify us by emailing [eprints@whiterose.ac.uk](mailto:eprints@whiterose.ac.uk) including the URL of the record and the reason for the withdrawal request.

Contents lists available at [ScienceDirect](https://www.sciencedirect.com)

# Atmospheric Environment: X

journal homepage: [www.journals.elsevier.com/atmospheric-environment-x](http://www.journals.elsevier.com/atmospheric-environment-x)

## Mobile monitoring reveals congestion penalty for vehicle emissions in London

Shona E. Wilde<sup>a</sup>, Lauren E. Padilla<sup>b</sup>, Naomi J. Farren<sup>a</sup>, Ramón A. Alvarez<sup>b</sup>, Samuel Wilson<sup>a</sup>, James D. Lee<sup>a</sup>, Rebecca L. Wagner<sup>a</sup>, Greg Slater<sup>c</sup>, Daniel Peters<sup>b</sup>, David C. Carslaw<sup>a,\*</sup>

<sup>a</sup> Wolfson Atmospheric Chemistry Laboratories, University of York, YO10 5DD, United Kingdom

<sup>b</sup> Environmental Defense Fund, 18 Tremont Street, Boston, MA, 02108, United States

<sup>c</sup> Environmental Defense Fund Europe, 3rd Floor, 41 Eastcheap, London, EC3M 1DT, United Kingdom

### ARTICLE INFO

#### Keywords:

Mobile monitoring  
Vehicle emissions  
Emissions ratio  
Congestion  
Quantile regression

### ABSTRACT

Mobile air pollution measurements have the potential to provide a wide range of insights into emission sources and air pollution exposure. The analysis of mobile data is, however, highly challenging. In this work we develop a new regression-based framework for the analysis of mobile data with the aim of improving the potential to draw inferences from such measurements. A quantile regression approach is adopted to provide new insight into the distribution of NO<sub>x</sub> and CO emissions in Central and Outer London. We quantify the emissions intensity of NO<sub>x</sub> and CO ( $\Delta\text{NO}_x/\Delta\text{CO}_2$  and  $\Delta\text{CO}/\Delta\text{CO}_2$ ) at different quantile levels ( $\tau$ ) to demonstrate how transient high-emission events can be examined in parallel to the average emission characteristics. We observed a clear difference in the emissions behaviour between both locations. On average, the median ( $\tau = 0.5$ )  $\Delta\text{NO}_x/\Delta\text{CO}_2$  in Central London was 2x higher than Outer London, despite the stringent emission standards imposed throughout the Ultra Low Emissions Zone. A comprehensive vehicle emission remote sensing data set ( $n \approx 700,000$ ) is used to put the results into context, providing evidence of vehicle behaviour which is indicative of poorly controlled emissions, equivalent to high-emitting classes of older vehicles. Our analysis suggests the coupling of a diesel-dominated fleet with persistently congested conditions, under which the operation of emissions after-treatment technology is non-optimal, leads to increased NO<sub>x</sub> emissions.

### 1. Introduction

Despite tailpipe emissions from road transport falling dramatically over the last 30 years due to the combined effect of increasingly stringent regulations and technological improvements in engine design and emissions control systems, the road transport sector still remains the largest contributor to nitrogen oxide (NO<sub>x</sub> = NO + NO<sub>2</sub>) emissions in both the UK (Department for Environment Food & Rural Affairs, 2022) and US (Office of Air Quality Planning and Standards, 2017). Moreover, in the newest update published by the World Health Organization, the annual guideline level of NO<sub>2</sub> was reduced by 75% to 10  $\mu\text{g m}^{-3}$ , which adds additional pressure to continue to reduce emissions (Organization, 2021). As such, there remains a need to monitor and improve the current understanding of on-road emissions, particularly as the characteristics of the vehicle fleet continue to change.

Mobile monitoring is increasingly used to assess the spatial variability of air pollution at high resolution. By mounting fast-response

instrumentation to a moving platform, spatial gradients in air pollutant concentrations can be illuminated and emissions sources that cannot be resolved through stationary monitoring can be revealed. For example, high resolution maps, which reveal “average” patterns in concentrations, can be derived either through route-based studies at the neighborhood level (Hu et al., 2012; Cummings et al., 2021), or through dense sampling of an entire area (Apte et al., 2017; Chambliss et al., 2020). Mobile monitoring has also been used to assess personal exposure (Berghmans et al., 2009; Boogaard et al., 2009), develop land-use regression models (Hankey and Marshall, 2015) or to assess the spatial representativeness of fixed monitoring networks (Zhu et al., 2020; Li et al., 2019). In addition, some studies have focused on the identification of pollution “hot-spots”, which are generally attributed to urban point sources in close proximity to the elevated concentrations (Chen et al., 2022; Miller et al., 2020).

Mobile monitoring platforms are also useful to assess emissions from mobile sources, in particular for the determination of vehicle emission

\* Corresponding author.

E-mail addresses: [shona.wilde@york.ac.uk](mailto:shona.wilde@york.ac.uk) (S.E. Wilde), [david.carslaw@york.ac.uk](mailto:david.carslaw@york.ac.uk) (D.C. Carslaw).

<https://doi.org/10.1016/j.aeoa.2024.100241>

Received 4 July 2023; Received in revised form 11 November 2023; Accepted 27 January 2024

Available online 9 February 2024

2590-1621/© 2024 The Authors. Published by Elsevier Ltd. This is an open access article under the CC BY license (<http://creativecommons.org/licenses/by/4.0/>).

factors in real world environments. “Plume-chase” methods can be employed to establish fuel-based emission factors of individual vehicles (Zavala et al., 2009; Hudda et al., 2013; Olin et al., 0), whilst non-targeted monitoring can be used to provide “fleet-averaged” emission factors (Zavala et al., 2006; Larson et al., 2017; Wen et al., 2019). Emission factors are typically estimated based on the concentration ratio of the target pollutant (e.g. NO<sub>x</sub>) to CO<sub>2</sub>, which represents the magnitude or intensity of emissions, independent of the total number of sources. By introducing a spatial component to the measured emission ratios, mobile measurements can provide valuable insight into the emissions behaviour of vehicles, which is crucial for guiding policy decisions, tracking progress in emission reduction efforts and evaluating the accuracy of emission inventories.

The calculation of emission ratios from ambient measurements recorded by a mobile platform is non-trivial. A possible approach is to calculate the ratio at each point in time (every second) as the quotient of enhancements in a target and tracer species, for example  $\Delta\text{NO}_x/\Delta\text{CO}_2$ . An aggregation step is then required to obtain a single value which represents the average emission ratio for the chosen domain, for example unique road segments (Sun et al., 2017; Padilla et al., 2022). Aggregating the data in this way reveals spatial detail but may be sensitive to outliers and discards information about the variance of the underlying data. An alternative approach, commonly implemented for source identification is to calculate the ratio using a linear regression (Wilde et al., 2021; Gilman et al., 2013; Salmon et al., 2018; Yacovitch et al., 2014). A regression has the benefit of providing a measure of the strength and significance of the relationship as opposed to just the direct ratio of increments. Through the combination of regression models with mobile data, there is the potential to provide a robust method to calculate spatially-varying emission ratios. Moreover, within a single framework, various types of regression models can be employed to maximise the information derived from mobile monitoring data.

Our chosen study area of London, UK, is of considerable interest from a road vehicle emissions perspective. The third largest city in Europe has a long history of developing policies to improve air quality through traffic management. London first implemented a low emission zone (LEZ) in 2008, targeting commercial vehicles and particulate matter reduction. In April 2019, the Ultra Low Emission Zone (ULEZ) was introduced in Central London, covering the same area as the Congestion Charge Zone (CCZ, introduced in 2003), before a further expansion to an area within the outer ring road was implemented on the 25th October 2021. The ULEZ effectively mandates that light and heavy duty diesel vehicles comply with the most recent emissions legislation (Euro 6 and Euro VI, respectively) and that gasoline cars and vans meet at least Euro 4 standards (post-2006). The ULEZ is also expanding from 29 August 2023 across all London boroughs. The progressively increased restrictions of these low emission zones has led to decreases in the concentrations of pollutants such as NO<sub>x</sub> and NO<sub>2</sub> according to the Greater London Authority (Greater London Authority, 2022). However, the emissions behaviour of vehicles operating inside the ULEZ is not monitored and consequently not well-understood.

In spite of the increasingly stringent air pollution regulations, London still suffers from poor air quality (Font et al., 2019; Shoari et al., 2022) and extreme congestion (TomTom Traffic Index, 2023). The success of current and future policies relies on the real-world emissions of new vehicles being lower than the ones they replace. In particular, controlling NO<sub>x</sub> emissions from diesel vehicles poses a technical challenge and requires innovative technology to reduce emissions to meet the thresholds required by the Euro 6/VI standard. In the European market, selective catalytic reduction (SCR) is the most prevalent technology for the control of NO<sub>x</sub> emissions from light and heavy duty diesel vehicles (Yang et al., 2015). SCR is most efficient in reducing NO<sub>x</sub> within a specific temperature range (typically between 250 °C and 400 °C) (Li et al., 2011). At engine temperatures below this range, which occur during cold starts or at low driving speeds associated with congestion, SCR has a lower capability to reduce NO<sub>x</sub> (Gao et al., 2021; Xu et al.,

2019). In Central and Inner London, where there is a high proportion of diesel fuel use, these factors combine to present a challenging set of conditions to effectively control emissions, which may limit the success of policies such as the ULEZ. Therefore, a study evaluating the emissions characteristics of vehicles is timely.

The principal aim of the current study is to leverage mobile monitoring data to reveal insights about the underlying emission sources. Specifically, we develop a new, regression-based method, which can be applied to mobile measurement data to calculate ambient emission ratios. We calculate ratios of  $\Delta\text{NO}_x/\Delta\text{CO}_2$  and  $\Delta\text{CO}/\Delta\text{CO}_2$  as a measure of the intensity of emissions sources, which cannot be established from ambient concentrations alone. The new method is applied to mobile measurement data in London (UK), where the aim is to quantify and contrast two areas of London with different emissions behavior. We use a quantile regression method to reveal more about the distribution of emissions spatially than is possible with simpler methods. Finally, we compare the mobile results with extensive vehicle emission remote sensing data to suggest that the real-world NO<sub>x</sub> emissions of vehicles operating inside the ULEZ can be substantially higher than the certified limits.

## 2. Materials and methods

### 2.1. Measurement platform

Mobile measurements were made using an instrumented mobile laboratory (Fig. S1) (Wagner et al., 2021). The instrumentation is housed in the load-space of a Nissan NV400SE transit van and air is sampled from a forward-facing inlet mounted 2.25 m above the ground near the front of the van to minimise self-sampling of exhaust emissions. Self-sampling can potentially occur during stationary intervals or when the motion of the van is in the direction of the exhaust. As such, stationary tests were carried out prior to the monitoring campaign, and indicated minimal instances of self-sampling from the exhaust. All enhancements observed during these tests corresponded to passing vehicles. However, periods where the van was parked or reversing were excluded from the analysis as a precautionary measure.

The instruments are powered by two 12VDC 230 Ah batteries which are either charged whilst driving by a 240 VAC inverter or by an external mains power socket when stationary. Geographical location, speed over ground, and vehicle direction is measured using a Garmin GPS 18x PC externally mounted at a height of 2.5 m. Data is collected at a resolution of 1 s via a computer equipped with custom DAQFactory software. Video footage was recorded using a VANTRUE X4S 4K Dash Camera mounted on the front wind screen, configured to capture one photograph per second.

The mobile laboratory is instrumented with a variety of fast-response analysers for multiple air pollutants, including methane (CH<sub>4</sub>), carbon dioxide (CO<sub>2</sub>), nitrogen oxides (NO<sub>x</sub>), ozone (O<sub>3</sub>), carbon monoxide (CO), sulphur dioxide (SO<sub>2</sub>) and particulate matter (PM). Response times were characterised based on the mixing ratio or concentration peaks identified through a series of flame ignition tests performed daily at the sample inlet before monitoring began. The data from each instrument were time-aligned by calculating the optimum offset for each species relative to the instrument with the fastest response time using a cross-correlation procedure. CO<sub>2</sub> was chosen as the reference measurement and the time series for each species was shifted according to the lag time which produced the maximum correlation coefficient with CO<sub>2</sub>. A standard offset of 5 s was then applied to the data to account for the delay caused by air travelling from the inlet to the instruments. The data were merged to geographical coordinates after the time alignment adjustment. For typical vehicle speeds of 20–30 mph this corresponds to a spatial resolution of approximately 50 m.

We applied a “snapping” procedure to correct inaccurate GPS observations resulting from the loss or reduction of signal. This was more problematic in Central London due to the high density of tall buildings.

We projected every GPS observation to the nearest point on the road network using only the road links that were included in the routes. Data points that were transformed more than 200 m were excluded from the analysis as an accurate location could not be verified.

Our analysis considers the measurements of  $\text{NO}_2$ ,  $\text{NO}_x$  ( $\text{NO} + \text{NO}_2$ ),  $\text{CO}_2$  and  $\text{CO}$ . Both  $\text{NO}_x$  and  $\text{CO}_2$  were measured using an Iterative Cavity enhanced Differential Optical Absorption Spectrometer (ICAD), developed by Airyx (Horbanski et al., 2019). The instrument provides a direct measurement of  $\text{NO}_2$ , which is measured in the spectral range between  $\approx 430$  and  $465$  nm. The absorption structure of  $\text{NO}_2$  is directly identified and separated from other overlapping absorptions (such as water vapour or glyoxal) by measuring the absorption spectrum and applying the ICAD algorithm. This allows direct  $\text{NO}_2$  measurements without interference of other substances or the need of a drying mechanism, which can introduce new interferences. The ICAD system relies on characteristic differential absorption structures, rather than absolute intensities and therefore is insensitive to temperature variations, vibrations and light source degradation. An internal converter based on gas phase titration with a  $\text{NO}_x$ -free  $\text{O}_3$  source converts  $\text{NO}$  to  $\text{NO}_2$  and allows for the measurement of total  $\text{NO}_x$ . Parallel  $\text{CO}_2$  measurements are made using a smartGAS Non-Dispersive Infra-Red (NDIR) gas sensor (F3-212205-05000). The instrument has a response time of 2 s in the standard configuration. Therefore, a linear interpolation was applied to the raw data to produce a 1 s time series.

$\text{CO}$  was measured using an Aerolaser AL5002  $\text{CO}$  Monitor, which provides an ultra fast measurement of  $\text{CO}$  with a response time of  $< 1$  s. The detection of  $\text{CO}$  is based on vacuum ultraviolet fluorescence, which employs the excitation of  $\text{CO}$  at a wavelength of around 150 nm (Gerbig et al., 1999). The excitation light is generated by a resonance  $\text{CO}_2$  lamp, which requires a supply of gas (0.26%  $\text{CO}_2$  in Ar) at  $50 \text{ mL min}^{-1}$ . The optical filter was continuously flushed with dry  $\text{N}_2$  at  $35 \text{ mL min}^{-1}$ . Calibrations were performed at the start and end of each drive period

using an in-built zero gas source and a reference gas standard containing a known amount of  $\text{CO}$ .

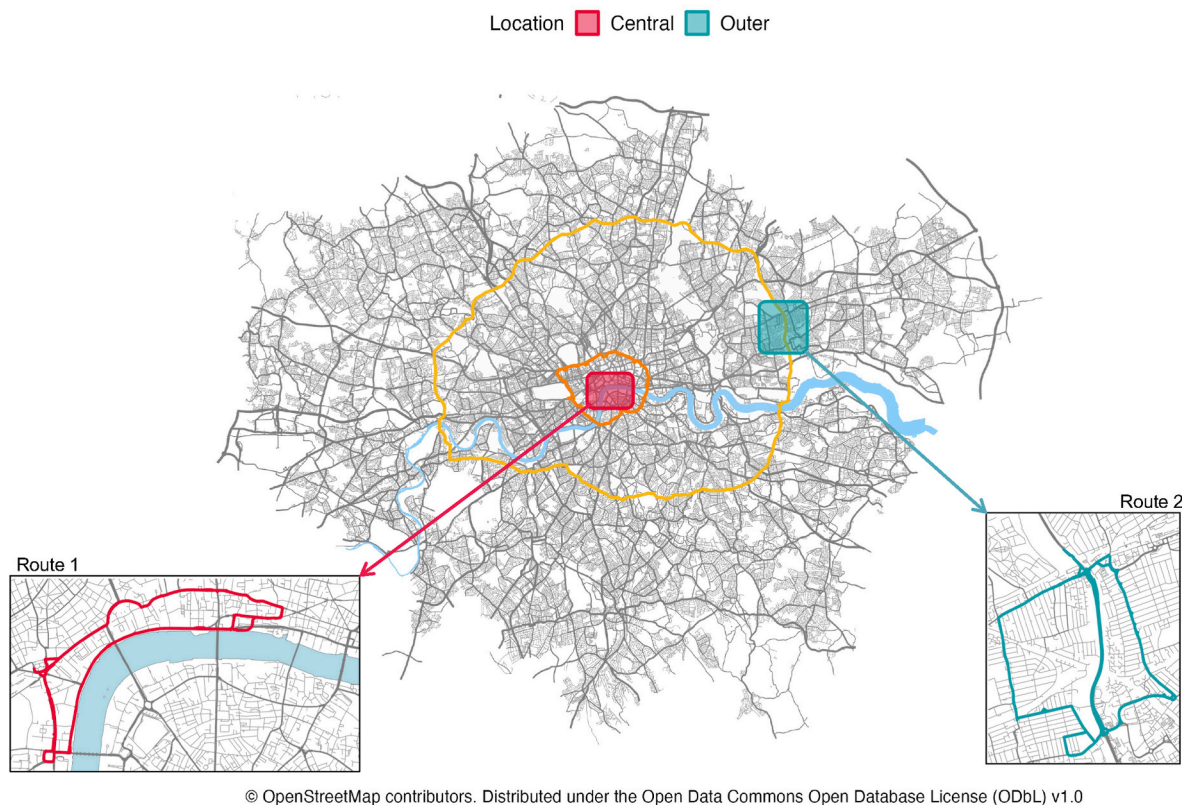
## 2.2. Measurement location

A mobile monitoring campaign was conducted in London, UK from 4th September 2022 to 15th September 2022. Sampling was predominantly performed in daytime and weekday hours between 08:00–20:00 local time for operational reasons. Fixed routes were defined in two locations prior to the campaign (Fig. 1). The routes were designed to cover a range of road types, traffic conditions and fleet mixes, in addition to sampling road links both inside and outside of the ULEZ.

Route 1 was a loop 8 km long in the middle of Central London, close to the River Thames. The route featured major roads, which form part of key bus routes, including Victoria Embankment, Trafalgar Square and The Strand. The entirety of the route was located in both the CCZ and ULEZ, where vehicle emissions are expected to be well controlled. Despite this, Padilla et al. (2022) found that this area was associated with high  $\text{NO}_2$  concentrations concurrent with elevated  $\Delta\text{NO}_x/\Delta\text{CO}_2$  ratios and had a high probability of exceeding the UK legal limit on  $\text{NO}_2$ .

Route 2 was a loop of 13 km in a residential area of Outer London. The route straddled the boundary of the ULEZ and predominantly featured arterial roads with a small section of residential roads. The route featured two similar high streets, one of which was inside the ULEZ, separated by a 2.5 km stretch of the North Circular, a major highway which encircles Central London.

Each route was repeated on a continuous cycle in alternate directions. High temporal coverage was given preference over the increased spatial coverage gained by longer routes in order to capture the range of conditions experienced in each location, particularly to ensure monitoring covered the variation in traffic intensity throughout the day. By performing targeted surveys with a high number of passes,



© OpenStreetMap contributors. Distributed under the Open Data Commons Open Database License (ODbL) v1.0

**Fig. 1.** Central and Outer London sampling locations within the Greater London boundary. The insets show the two sampling routes. The orange and yellow lines represent the boundary of the Congestion Charge Zone (CCZ) and Ultra Low Emissions Zone (ULEZ) at the time of the September 2022 monitoring campaign, respectively. (For interpretation of the references to colour in this figure legend, the reader is referred to the Web version of this article.)

we sought to reduce the large uncertainty in the median estimate of concentrations and emissions intensity, which arises in studies with far less drives (Padilla et al., 2022; Chen et al., 2022). In total, 47 and 41 loops were completed in Central and Outer London respectively, with an approximate 50:50 split in the clockwise and anti-clockwise directions. A total of 103,928 data points were collected in Central London and 101,342 in Outer London.

### 2.3. Additional data sets

#### 2.3.1. Remote sensing

Vehicle emission remote sensing (RS) measurements were used to supplement the mobile monitoring data. RS is a non-intrusive roadside technique which uses infrared and ultraviolet absorption spectroscopy to quantify the concentration of pollutants in the exhaust plumes of passing vehicles (Bishop et al., 1996; Burgard et al., 2006). Typically, the measured RS concentration values are reported as molar volume ratios of pollutants to CO<sub>2</sub>, which can be directly compared to mobile monitoring data. RS also reports the associated technical information (e. g., vehicle age, fuel type, emissions standard) for each vehicle measurement. This is achieved through the use of a registration plate camera alongside the spectroscopic apparatus, and allows for the aggregation of the emissions data to generate average values for different vehicle groupings.

A considerable amount of RS data has been collected across the UK over the past decade, spanning a wide range of site locations and ambient conditions (Farren et al., 2020; Davison et al., 2021). The RS data set used in this work is unique in both its size and coverage, consisting of 681,187 valid vehicle measurements obtained between 2012 and 2022 from 77 urban UK sites. To generate values for useful comparison with mobile measurements data, the RS molar volume ratios of NO<sub>x</sub>/CO<sub>2</sub> within the data were grouped by vehicle type, fuel type, and Euro emission standard type, and aggregated to produce a mean value per vehicle group.

#### 2.3.2. Vehicle counts

Traffic estimates for unique road links were acquired from the Department for Transport (2021). Vehicle counts representing the number of vehicles that travel past the count point (in both directions) on an average day of the year for count points located on or within 100 m of the measurement routes were obtained. Count data from 2021 was used as this was the most recent data set. However, we recognise that this may be an underestimation for 2022 as traffic volume continued to rebound following the COVID-19 pandemic. There were 14 and 12 unique counting points distributed across route 1 and route 2, respectively (Fig. S2).

### 2.4. Calculation of emission ratios

Emission ratios provide a way of linking the measured ambient mixing ratios to emissions. Simultaneous, high frequency measurements of a pollutant and a tracer species, such as CO<sub>2</sub>, enable the calculation of the emissions intensity, which represents the amount of pollutant emitted per unit of fuel burned. The emissions intensity is a useful quantity because it can be related to direct emission measurements made at the exhaust using RS detectors or Portable Emissions Measurement Systems (PEMS) (Carslaw and Rhys-Tyler, 2013; Smit et al., 2021). Such systems provide disaggregated, vehicle specific emissions estimates and ratios, which can be used to understand how emissions relate to individual vehicle models or manufacturers, as well as investigating the effectiveness of emission control technologies and legislation (Carslaw et al., 2015; Grange et al., 2020). Mobile emission ratios are inherently different, because the measurements describe a mixture of the most recently emitted plumes, likely from the vehicle immediately in front of the mobile platform and older, more dispersed emissions from vehicles further up (or down) the road in addition to nearby point

sources. Therefore mobile emission ratios can be interpreted as the combined characteristics of the vehicle fleet (and non-vehicle sources), representative of the fleet composition and the operating conditions of the vehicles, the latter of which can be influenced by a wide range of real-world conditions such as traffic state and ambient temperature (Grange et al., 2019).

#### 2.4.1. Background subtraction

The calculation of emission ratios requires the definition and calculation of background mixing ratios for each species; a common challenge in the analysis of mobile data. Short-term studies often apply background corrections to account for temporal variation in the regional background, which can vary on timescales shorter than a day due to boundary layer mixing conditions (Chen et al., 2022). Data-rich studies commonly featuring more than 10 unique sampling days have found this temporal uncertainty to be relatively small in comparison to the sampling precision and hence do not always perform background adjustments (Miller et al., 2020). In this study we seek to isolate the local exhaust component of the measurements by separating the most recently emitted plumes from the urban background. In this case, the background mixing ratios represent a level of well-mixed pollution made up of both “aged” local emissions emitted well before the time of the measurement, and emissions transported to the measurement location from outside the immediate vicinity. For a species *X*, once subtracted the remaining enhancement ( $\Delta X$ ) is then attributed to fresh, local emissions, mainly from road transport or nearby non-road sources.

To perform the background subtraction we apply the concept outlined by Padilla et al. (2022), where the background mixing ratios were calculated as the 1st percentile measurement in a rolling 5-min, centered window on the mobile time series, which included all data 2.5 min before and after each 1 s measurement. The rolling-percentile method does not detect local exhaust plumes, rather assumes the baseline of the time series is representative of the background. The choice of background parameters, such as percentile level and window length can have implications for the derived emission ratios. We chose the 1st percentile to ensure the smallest plumes, which arise due to sampling of the lowest-emitting vehicles or because they were relatively well-dispersed at the time of measurement are not excluded from the analysis. Sensitivity tests revealed that the choice of rolling window width did not significantly affect the derived emission ratios (Fig. S3). This is an important result as it means the derived emissions ratios can be robustly compared to ratios obtained from other methods such as remote sensing. More detail about the background calculation and sensitivity analysis can be found in the Supplementary Information.

#### 2.4.2. Distance-weighted quantile regression

We implement a regression-based approach to calculate emission ratios of  $\Delta\text{NO}_x/\Delta\text{CO}_2$  and  $\Delta\text{CO}/\Delta\text{CO}_2$ . All data processing was carried out using the R programming language (R Core Team, 2022) and the functions used to perform the regression analysis are available in the **mobilemeasr** R package (Wilde, 2021). Emission ratios were calculated using distance-weighted quantile regression centered at fixed points located every 10 m along each monitoring route. This was selected as an appropriate resolution, given that at an average speed of 20 mph the monitoring platform would cover a distance of 9 m in a second.

From an emissions perspective, quantile regression allows the typically skewed nature of on-road vehicle emissions, caused by a small number of gross emitters to be examined (Gary A. Bishop and Lawson, 2012; Collet et al., 2015). Unlike ordinary least squares (OLS) regression, which focuses on a single mean dependent variable response, quantile regression can quantify the relationship (slope) between the explanatory variable(s) and any quantile ( $\tau$ ) of the response variable from the median to the tails, recognizing that these relationships are not necessarily the same across the whole distribution of the response variable (Buchinsky, 1998). For example, Fig. S5 shows the slope between  $\Delta\text{NO}_x/\Delta\text{CO}_2$  increases along with  $\tau$ , indicating that the highest NO<sub>x</sub>

mixing ratios are associated with more intense emissions and are not just an artifact of a changing intercept. In a physical sense, this reflects the large variability in emissions resulting from a broad spectrum of vehicles operating under various conditions.

We discuss emission ratios for two values of  $\tau$ ;  $\tau = 0.5$  and  $\tau = 0.99$ . We consider  $\tau = 0.5$  as the fleet-average emission intensity, which represents the typical fleet composition and prevailing traffic conditions at each point. In contrast, the relationship between enhancements of  $\text{NO}_x$  and  $\text{CO}_2$  at the upper portion of the distribution ( $\tau = 0.99$ ) reveals the characteristics of the highest emitters. Implementing quantile regression in this way allows transient features associated with high emitters to be explored independently of the typical emission characteristics of a location, which would not be possible using OLS alone. Comparing emission intensities at these two different quantiles along routes with different driving conditions and fleet composition is the key to estimating a congestion penalty on vehicle emissions.

Using  $\text{NO}_x$  as an example, the conditional quantile of the response variable  $Q_\tau(\Delta\text{NO}_x)_i$ , for the  $i$ th observation was calculated using Equation (1), where  $\beta_1$  is the quantile-specific regression coefficient and  $\beta_0$  is the intercept.

$$Q_\tau(\Delta\text{NO}_x)_i = \beta_0(\tau) + \beta_1(\tau) \cdot \Delta\text{CO}_2_i \quad (1)$$

The  $\beta$  coefficients are found by minimising the quantile loss function, known as the median absolute deviation (MAD). The MAD is shown by Equation (2), where  $\omega_i$  represents the distance weight assigned to the  $i$ th observation, reflecting its position relative to the central regression point, and  $\rho_\tau$  is the check function (Equation (3)) for residual  $u$ , which gives asymmetric weights to the positive and negative differences between the observed and predicted values based on the chosen quantile level  $\tau$ .

$$\text{MAD} = \frac{1}{n} \sum_{i=1}^n \omega_i \rho_\tau(\Delta\text{NO}_x)_i - Q_\tau(\Delta\text{NO}_x)_i \quad (2)$$

$$\rho_\tau(u) = \begin{cases} \tau \cdot u, & \text{if } u \geq 0 \\ (1 - \tau) \cdot u, & \text{if } u < 0 \end{cases} \quad (3)$$

The distance weights ( $\omega_i$ ) were determined at each point using a Gaussian kernel within a continuous moving window described by Equation (4), where:  $K(x, x')$  represents the value of the Gaussian kernel,  $\|x - x'\|^2$  is the squared Euclidean distance between the regression point  $x$ , and observation  $x'$ , and  $\sigma$  is the standard deviation that controls the width of the Gaussian curve. The Gaussian kernel assigns higher weights to observations that are closer to the regression point while decreasing the weights as the distance increases. In reality, concentration measurements at any specific location are more strongly influenced by nearby emissions and less by distant sources, which this approach reflects. The geographical weighting allows spatial patterns to be illuminated whilst minimising the noise of outliers in calculating the slope of the best fit line, which represents the emissions ratio, by including all observations from all passes in each regression. (Or in this case, for computational efficiency, only observations with a relative weight of  $> 1\%$  were used to fit the quantile regression models.) Our approach is novel compared to existing methods, which calculate a ratio based on the division of two average values and use a discrete step function to assign weights to observations within fixed road segments based on a binary classification, where the weighting takes a value of 1 inside the segment and 0 outside (Sun et al., 2017; Padilla et al., 2022).

$$K(x, x') = \frac{1}{\sqrt{2\pi}\sigma} \exp\left(-\frac{\|x - x'\|^2}{2\sigma^2}\right) \quad (4)$$

The spatial scale over which the original data is aggregated can be controlled by varying the width of the kernel and can be thought of as similar to varying the length of discrete road segments.  $\sigma$  can be adjusted according to the use-case. For example, a small  $\sigma$  (20 m) and hence narrow Gaussian can be used to focus on localized effects at a fine spatial

scale. A large value of  $\sigma$ , such as 500 m, extends the range over which measurements influence the regression and would therefore be useful in studying emission patterns on a broader, regional scale (Fig. S6). In this analysis,  $\sigma$  was set at 100 m to represent a near-field distance scale, where direct exposure to vehicle emissions is likely to occur (Watson et al., 1988).

Implementing regression in this way offers great flexibility as the type of regression model can be varied to suit the cause. Weighting variables can be included in different regression approaches such as ordinary linear regression and generalized additive models, in addition to machine learning models such as random forests. Additionally, there are countless potential variables that can be built into a specific model to perform quantitative analysis using mobile measurements that would not be possible using existing methods.

## 2.5. Mean mixing ratios

Mean mixing ratios of  $\text{NO}_x$ ,  $\text{NO}_2$  and  $\text{CO}_2$  were calculated at 10 m points on the road network using a two-step approach. First, the mean mixing ratio at each point was calculated for every individual circuit of the identical route using a distance-weighted mean. This is similar to a drive-pass mean as outlined in Apte et al. (2017); Miller et al. (2020) and prevents the over-weighting of measurements made in the same location when the van was stationary or moving at very low speeds. The observation-weights were calculated using a Gaussian kernel (4) as in 2.4.2 with a  $\sigma$  value of 100 m, (consistent with the emission ratio calculation). Second, the circuit means for each point were aggregated using the arithmetic mean to give an overall mean mixing ratio.

## 3. Results and discussion

### 3.1. Spatial variation in emissions intensity

Distance-weighted quantile regression was performed at equally spaced 10 m points along each route. The  $\Delta\text{NO}_x/\Delta\text{CO}_2$  ratio, referred to as the emissions intensity, was extracted as the regression coefficient with  $\text{CO}_2$ , which was both significant and positive for 100% of models (each model represents the regression results for an individual 10 m point). All emission ratios are expressed as molar ratios and reported in  $\text{ppb ppb}^{-1}$ . We discuss emission ratios for two values of  $\tau$ ;  $\tau = 0.5$  and  $\tau = 0.99$  to yield insights about persistent and transient emission events, respectively. Locations where emission ratios are systematically elevated across the entire conditional distribution represent a persistent source of high intensity emissions associated with a specific location. These locations essentially represent emissions ‘‘hot spots’’, and may be used to inform the development of targeted policies to improve air quality. On the other hand, locations with an elevated emissions intensity at the highest quantiles, but which are not evident in the median ( $\tau = 0.5$ ), represent the most intense emission events, which may occur anywhere on the road network as a result of following directly behind a highly polluting vehicle. This is useful for identifying the subset of the fleet which may represent a small fraction of the overall fleet but contribute disproportionately to the total emissions. Owing to the difference in the source characteristics, the spatial patterns in the  $\Delta\text{NO}_x/\Delta\text{CO}_2$  ratio for  $\tau = 0.5$ , were not replicated for  $\tau = 0.99$ , (Fig. S7). Moreover, in both locations the emissions intensity increased with the quantile level,  $\tau$  (Fig. S8), demonstrating the wide distribution of emissions across a road network, which are most intense in the upper tail of the distribution due to a small fraction of high-emitting vehicles.

Fig. 2 shows the spatial pattern of the median emissions intensity, represented by  $\tau = 0.5$ , for the two measurement routes alongside the mean  $\text{NO}_x$  mixing ratio at each 10 m point. Despite the relatively small area of our study, there was considerable spatial variability in the emissions intensity across both routes due to localised variations in the fleet and traffic congestion. For example, the median map had a coefficient of variation (CV) of 0.15 and 0.24 in Central and Outer London,

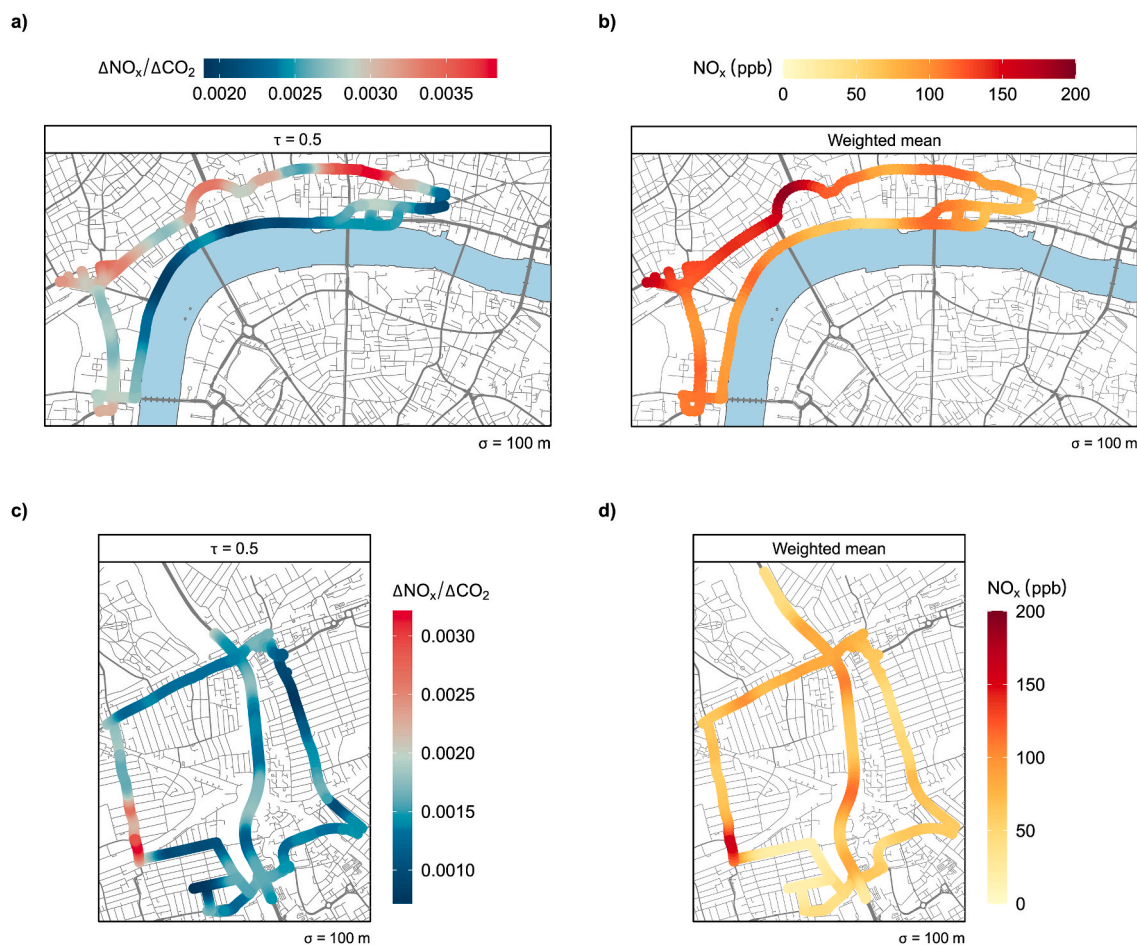


Fig. 2.  $\Delta\text{NO}_x/\Delta\text{CO}_2$  enhancement ratio calculated using distance-weighted quantile regression for  $\tau = 0.5$  and mean  $\text{NO}_x$  mixing ratio in Central London (a and b)) and Outer London (c and d)). Note the unique colour scale for each sub-figure. Map data © OpenStreetMap contributors. Distributed under the Open Data Commons Open Database License (ODbL) v1.0. (For interpretation of the references to colour in this figure legend, the reader is referred to the Web version of this article.)

respectively. A clear pattern emerged in Central London, where the median emission intensity was consistently elevated along the northern section of the route, compared to the southern section along the Thames Embankment. To further illustrate the differences between road links, we compare two transects, each approximately 2.5 km in length (Fig. S9). The median  $\Delta\text{NO}_x/\Delta\text{CO}_2$  ratio along the north transect was 0.0031, which was  $1.32 \times$  higher than the south transect. This was consistent with the mean  $\text{NO}_x$  mixing ratios, which were also  $1.32 \times$  higher on the north transect. Differences in these two transects are likely due to the prevailing traffic conditions and fleet composition. The north transect experienced moderately higher levels of congestion, where the average speed was  $9 \text{ km h}^{-1}$  compared to  $12 \text{ km h}^{-1}$  on the south transect. Additionally, the traffic counts reveal a clear difference in the fleets across the two transects (Fig. S10). The average annual daily traffic counts were 25% lower for the north transect, as expected due to the slower moving traffic. However, the higher emissions intensity suggests a greater emission per vehicle. The most notable difference was the contribution of buses to the total counts along each transect. On average, along the south transect, buses and coaches contributed only 2% to the total counts. However, this was 12% for the north transect. Despite the lower number of total counts on the north transect, the mean daily count of buses and coaches was  $5 \times$  higher; 1755 and 371 for the north and south transect, respectively, indicating that ambient mixing ratios can be influenced by the strength of emissions sources rather than the quantity of sources. There was also fine-scale variability along the north transect, where the values varied up to 1.5 times within only a few hundred metres. The most intense emissions were sampled at the north-

east section of the route centered on a typically congested intersection. High values were also observed along Aldwych, a semi-circular road link at the centre of the north transect where there are short distances between traffic lights and two lanes of traffic in each direction.

In Outer London, the most prominent feature in the emissions intensity for  $\tau = 0.5$  was an enhanced region along the western edge of the route. The area of enhancement was also mirrored in the mean mixing ratio (Fig. 2d). This location features traffic lights at a narrow intersection and was often congested with queuing traffic in both directions. As a result, the average speed was the lowest of anywhere along the route, averaging less than  $10 \text{ km h}^{-1}$ . Additionally, there were often sequences of acceleration and deceleration, which when travelling in the anticlockwise direction (south), were coupled with a positive road gradient.

The spatial patterns in the median emissions intensity reveal persistent hot spots, which in both Central and Outer London, were locations which experienced low vehicle speeds and heavy congestion. In general, the degree of congestion in Central London was much greater, reflected in the mean speed (subsection 2.5) of the mobile monitoring platform, which was  $10.7 \text{ km h}^{-1}$  compared to  $27.7 \text{ km h}^{-1}$  in Outer London. Moreover, the mean emissions intensity ( $\tau = 0.5$ ) was  $0.0028 \text{ ppb ppb}^{-1}$  in Central London, approximately twice as high as Outer London ( $0.0015 \text{ ppb ppb}^{-1}$ ), suggesting intense  $\text{NO}_x$  emissions are linked with the level of congestion. We term this a “congestion penalty”. This penalty also translated to the ambient  $\text{NO}_x$  mixing ratios, which were 1.6 times higher in Central London (Fig. 2). These findings illustrate how vehicle emissions in Central London remain elevated despite

the implementation of policies such as the ULEZ.

Congested conditions typically facilitate high  $\text{NO}_x$  emissions caused by the non-efficient operation of after-treatment systems (Lozhkina and Lozhkin, 2016). During stop periods there can be a significant cooling effect on catalysts due to low exhaust temperatures, which limit the ability of the catalyst to reduce  $\text{NO}_x$ . Furthermore, when operating at low speeds, the exhaust fails to generate sufficient heat, hindering the catalyst's ability to reach the necessary temperatures for efficient operation. This effect is especially relevant for diesel vehicles whose exhaust temperature is lower than petrol vehicles due to lean-burn characteristics, where the excess air acts to cool the system as it flows through (Gao et al., 2021). Therefore the combined effect of diesel vehicles and heavy traffic is likely to give rise to excess emissions of  $\text{NO}_x$ .

Although the share of new diesel car sales is declining in the UK, a substantial portion of the fleet continues to rely on diesel fuel, creating the potential for excess  $\text{NO}_x$  emissions. Passenger cars and private hire vehicles constitute 60% and 77% of the vehicle fleet in Central and Outer London, respectively (Fig. S14) (Greater London Authority, 2023), of which, approximately 40% were diesel in 2021 (Department for Transport, 2022). The remainder of the fleet is predominantly composed of light goods vehicles (LGVs), heavy goods vehicles (HGVs) and buses, all of which are almost exclusively powered by diesel engines (Greater London Authority, 2023). Consistent with Fig. 2, this effect is likely exacerbated in Central London, where there is a higher prevalence of LGVs and buses (Fig. S14) resulting in a greater proportion of diesel-powered vehicles compared to Outer London.

To expose differences between the two sampling locations, Fig. 3 shows the distribution of the  $\Delta\text{NO}_x/\Delta\text{CO}_2$  ratio for  $\tau = 0.5$  and  $\tau = 0.99$ . The values are plotted in ascending order for each quantile level. The range of values observed in Central London are shown by the dashed horizontal lines. For  $\tau = 0.5$ , the emissions intensity in Central London was higher than Outer London across the majority of the sampled road network, such that only the highest 5% of values in Outer London were within the range observed in Central London. This highlights the unique environment in Central London, where emissions are persistently elevated across the entire road network, despite the restrictions imposed by both the ULEZ and CCZ. A possible explanation is the presence of an intensely-emitting group of vehicles, consistently present only throughout the Central London sampling domain, or as a consequence of driving conditions which facilitate higher emissions.

Regarding the former, it's important to note that the ULEZ permits Euro 6/VI diesel vehicles which were certified before the EU's emissions type-approval procedure included real-driving emissions (RDE) tests.

These "pre-RDE" vehicles are those typically registered before 2020 and were subject to emissions testing using laboratory-based procedures, which often failed to accurately replicate real-world driving conditions. Consequently, this specific category of Euro 6 diesel cars, on average, has emissions five times higher than the officially regulated limits when driven under real-world conditions (The International Council on Clean Transportation, 2017). However, it's expected that pre-RDE vehicles are equally present in Outer London and are therefore not the key driver of the more intense emissions in Central London. Rather, these vehicles represent an additional subset of the fleet which are especially susceptible to excess  $\text{NO}_x$  emissions when coupled with traffic congestion.

Regarding the latter, even during periods of relatively low traffic volume (prior to 8 a.m. or after 6 p.m.), the average speed for a loop exhibited a minimal increase of less than  $2 \text{ km h}^{-1}$  compared to congested periods. This reflects the stop-start nature of driving in Central London, where a dense network of intersections, traffic lights, and pedestrian crossings prevents the establishment of free-flowing traffic necessary for the optimal functioning of emission control systems. Moreover, the region of most intense emissions in Outer London was also located inside the ULEZ but was associated with some of the lowest average speeds along the route, suggesting a localised prevalence of high emitting vehicles or that the enhanced emissions are due to persistent congested conditions.

For  $\tau = 0.99$  the mean emissions intensity was higher in Central London ( $0.012 \text{ ppb ppb}^{-1}$ ), compared to Outer London ( $0.009 \text{ ppb ppb}^{-1}$ ), however the spatial distribution was less variable in Central London ( $\text{CV} = 0.21$ ), suggesting there is a strong prevalence of high-emission events, which occur across the bulk of the road network. A much greater variation was observed in Outer London ( $\text{CV} = 0.62$ ), where 85% of the sampled network was either above or below the range observed in Central London. This suggests that high-emitting vehicles are less common, however the extreme, albeit infrequent emission events were typically associated with greater  $\Delta\text{NO}_x/\Delta\text{CO}_2$  ratios than in Central London. Fig. 3 highlights two main advantages of this method. First, adopting an emissions intensity approach yields information about the magnitude of the sources themselves since it is independent of traffic volume. Second, utilising quantile regression enables the simultaneous examination of transient events alongside the average emission characteristics of the sampling domain.

### 3.2. Interpretation of high-emission events

Traffic emissions are well approximated by a heavy-tailed

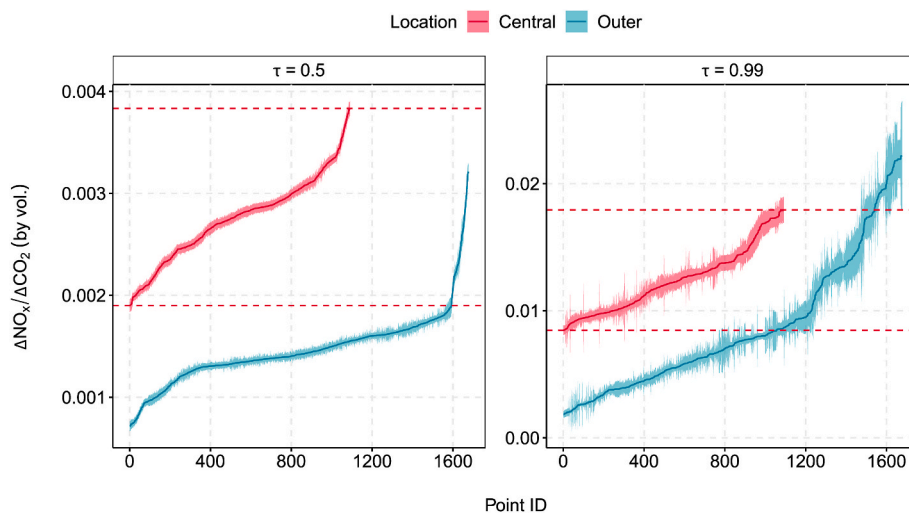


Fig. 3. Distribution of the  $\Delta\text{NO}_x/\Delta\text{CO}_2$  ratio in Central and Outer London where  $\tau = 0.5$  and  $\tau = 0.99$ . The x-axis represents the identifier for each 10-m point arranged in ascending order of emission intensity. The shading represents the standard error of the quantile regression coefficients. The dashed lines indicate the minimum and maximum values for Central London.

distribution due to the significant vehicle-to-vehicle variability, where a small population of high-emitters are responsible for a disproportional amount of the total emissions (Böhm et al., 2022; Bishop and Stedman, 2008). Therefore, methods which aid the identification and assessment of gross polluters are important for designing policy to reduce vehicle emissions. The 99th percentile ( $\tau = 0.99$ ) in quantile regression provides insights into the extreme values of the dependent variable and hence can be leveraged to identify the most intense emitters. We illustrate this, using Outer London as an example, where the maximum emissions intensity for  $\tau = 0.99$  exceeded that for Central London (Fig. 3) and where there is a greater possibility of uncontrolled emissions from vehicles due to the route's position outside the CCZ and on the boundary of the ULEZ.

The most intense emission events in Outer London were identified using Fig. 3 where the  $\Delta\text{NO}_x/\Delta\text{CO}_2$  ratio was above the Central London range for  $\tau = 0.99$  but below the Central London range for  $\tau = 0.5$ . This ensures only locations with intermittent intensity are included and not those with high values across the entire distribution, which represent a persistently intense source. Three distinct sections of road were identified through this process, covering four unique roads: Romford Road, Kempton Road, Ilford Lane and Fanshawe Avenue (Fig. S11). To gain further insight into the source of such events, the time series of unique drive passes along each road link were examined. Drive passes which featured spuriously large plumes of  $\text{NO}_x$  and hence warranted further investigation were identified by calculating the mean  $\text{NO}_x$  mixing ratio for each pass on each road link. Outliers were identified as those passes which were above  $1.5 \times$  the interquartile range of all the pass means (Fig. S12). In total 12 unique events were identified. Video footage providing continuous street level imagery was then used to assign a vehicle or source to each plume event. Of the 12 identified events, 8 corresponded to instances where the mobile monitoring platform was either directly following or passing a stationary bus or goods vehicle. An example screenshot from the dash camera is shown in Fig. S13. The remaining plumes were either attributed to passenger vehicles or could not be assigned to a specific source.

The root cause of such emissions can be further examined. A single example on Romford Road was used to illustrate this (pass 30 in Fig. S12). During this drive pass  $\text{NO}_x$  mixing ratios peaked at over 4000 ppb when following a TfL bus in slow moving traffic. The primary  $\text{NO}_2$  fraction was determined by calculating the total oxidant ( $\text{OX} = \text{NO}_2 + \text{O}_3$ )  $\text{OX}/\text{NO}_x$  slope (Clapp and Jenkin, 2001) for the single plume, which was found to be 64%.  $\text{NO}_2$  enhancements of this magnitude are only possible through the direct emission of  $\text{NO}_2$  because  $\text{NO}_2$  formation in the atmosphere (through the  $\text{NO} + \text{O}_3$  reaction) is limited by  $\text{O}_3$  availability. Much of the bus fleet in London is composed of retrofit vehicles, fitted with diesel particulate filters (DPF) and SCR systems. In both systems, Diesel Oxidation Catalysts (DOC) are used to convert  $\text{NO}$  (within  $\text{NO}_x$  emissions) to  $\text{NO}_2$ , which is then subsequently reduced by the SCR system (Richards et al., 2004). However, as previously commented on, in the congested conditions typical across London, the performance of the retrofitted units is poorer than in free-flowing conditions (Barratt and Carslaw, 2014). Hence, we emphasize the potential for intense emissions of  $\text{NO}_x$  and a higher proportion of primary  $\text{NO}_2$  due to the combined effect of retrofit buses operating in stop-start traffic conditions.

Whilst we acknowledge that video footage cannot conclusively link plume events to a particular vehicle, we highlight the possibility that there are a population of heavy duty diesel vehicles, in particular buses, which produce the most-intense emissions, something also concluded by previous studies (Tan et al., 2014; Zhou et al., 2020). This issue will be more significant in Central London, where there are a greater proportion of buses (Fig. S14), which may be responsible for driving up the emissions intensity in relation to Outer London, despite the implementation of strict vehicle emissions standards equivalent to Euro VI.

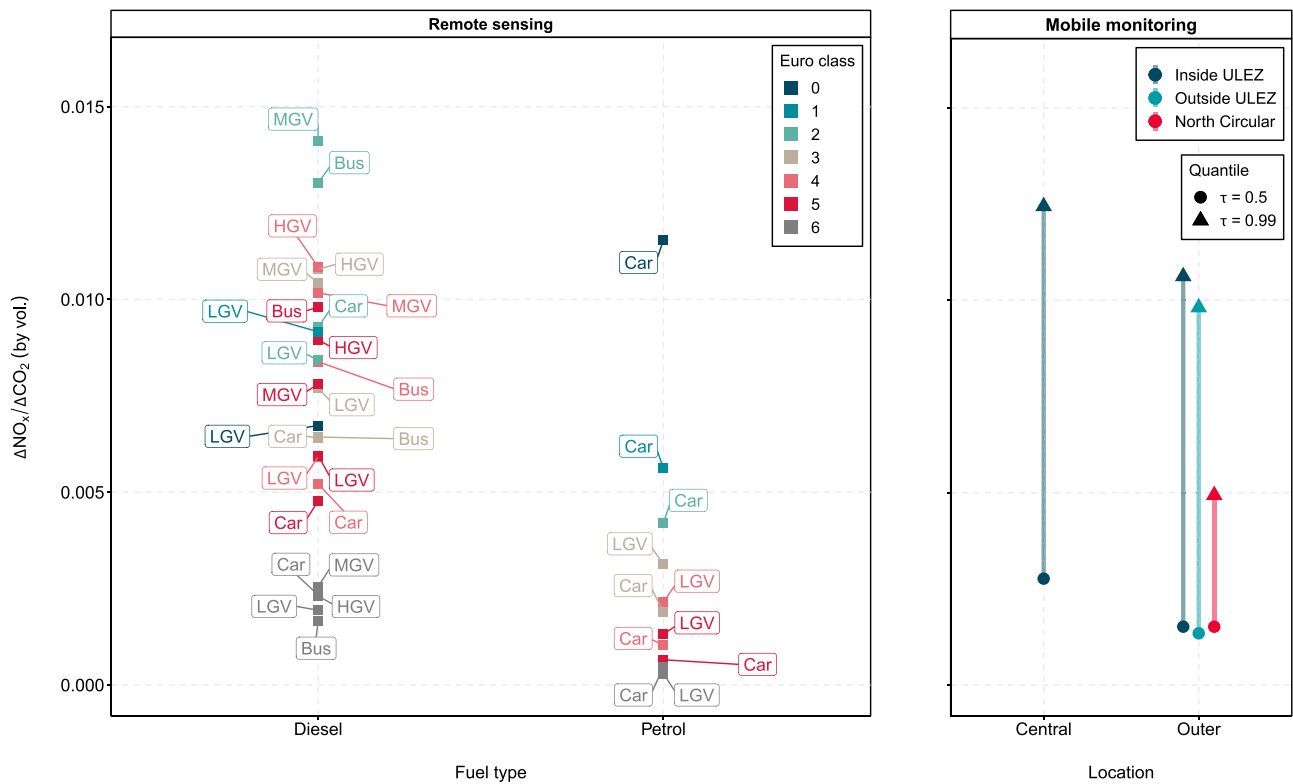
### 3.3. Comparison with remote sensing

The direct output of a RS measurement is the concentration of a given pollutant in the test vehicle's exhaust plume relative to the  $\text{CO}_2$  concentration, which can be compared to the ambient emission ratios derived from mobile monitoring. The RS measurements were collected in 77 urban locations across the UK. The data represent an average emission ratio under a range of operating conditions, where the variation within each group is driven by differences in manufacturer, vehicle age, vehicle speed and vehicle acceleration, in addition to external factors such as ambient temperature. RS measurements typically measure vehicles at moderate vehicle specific power (VSP), at speeds between 5 and 50  $\text{km h}^{-1}$  (Fig. S15). RS measurements are generally unable to capture the complete emissions behaviour, particularly in scenarios with slow vehicle speeds and stop-start traffic, which are frequently encountered in both Central and Outer London (Fig. S15). Mobile measurements have the potential to provide information about the emissions behaviour of the fleet under a wider set of conditions. However, comparison to RS observations is useful to determine whether the ambient ratios derived from mobile monitoring are consistent with the fleet-average ratios obtained from RS.

Fig. 4 shows the aggregated vehicle emission RS  $\Delta\text{NO}_x/\Delta\text{CO}_2$  ratio and  $\Delta\text{CO}/\Delta\text{CO}_2$  emission ratios, grouped by fuel type, vehicle type and European emission standard. Also shown are the mean ambient emission ratios across each mobile monitoring route for  $\tau = 0.5$  and  $\tau = 0.99$ , chosen to represent the distribution of emissions at each location. The Outer London route was further divided into three unique sections: Inside ULEZ, Outside ULEZ and the North Circular. Fig. 4 shows the range of ratios derived from mobile monitoring is within the extent of the remote sensing measurements. This information is valuable because it demonstrates the capability of mobile monitoring studies to provide policymakers with ambient ratios that help determine fleet characteristics in areas where comprehensive remote sensing (RS) measurements are lacking.

Considering Central London, where the route lies entirely within the ULEZ and therefore vehicles must meet the relevant standards (Euro 4 for petrol, Euro 6/VI for diesel and Euro 3 for motorbikes) or pay a fee. High compliance rates of up to 94% for the entire zone have been reported since the expansion in October 2022 (Greater London Authority, 2022). Therefore, owing to the high proportion of taxis and buses, it is expected that the emission ratios should be indicative of a low-emitting, Euro 6/VI diesel fleet. The route-mean ambient  $\Delta\text{NO}_x/\Delta\text{CO}_2$  ratio for  $\tau = 0.5$  was 0.0028, which was slightly higher than the RS range for Euro 6/VI diesel vehicles (0.0017–0.0026  $\text{ppb ppb}^{-1}$ ). The mean ambient  $\Delta\text{NO}_x/\Delta\text{CO}_2$  ratio for  $\tau = 0.99$ , representing the highest emitters, was 0.012  $\text{ppb ppb}^{-1}$ , which is analogous to the average emissions from vehicles which adhere to much lower Euro standards, such as Euro II buses. It is conceivable that there exists a small fraction of older, more polluting vehicles inside the ULEZ responsible for the high ratios. However, given the high level of compliance, our data suggests the behaviour of some Euro 6/VI vehicles becomes comparable to much older vehicles under the congested conditions in Central London. This finding is supported by Fig. S16, which shows the calculated quantiles of the  $\Delta\text{NO}_x/\Delta\text{CO}_2$  for Euro 6/VI diesel vehicles within the RS data. The median ( $\tau = 0.5$ ) ratio shows the emissions of Euro 6/VI vehicles are low compared to previous standards. However, the tail of the distribution reveals a proportion of vehicles which emit more intensely. For example, for  $\tau = 0.99$ , the RS  $\Delta\text{NO}_x/\Delta\text{CO}_2$  ratio for Euro VI buses was 0.01  $\text{ppb ppb}^{-1}$ , which is greater than the mean RS emission ratio of Euro III, IV, and V buses (Fig. 4a) but very similar to the route-mean ambient ratio at  $\tau = 0.99$  in Central London (Fig. S16). This is further evidence of the congestion penalty which prevents diesel vehicles in Central London from achieving Euro 6/VI equivalence, effectively reducing the emissions standard of the fleet (Fig. 4a). The consequence of the congestion penalty is a significant increase in the  $\text{NO}_x$  emissions of certain high-emission vehicles, raising them by a factor of five times above the

(a)



(b)

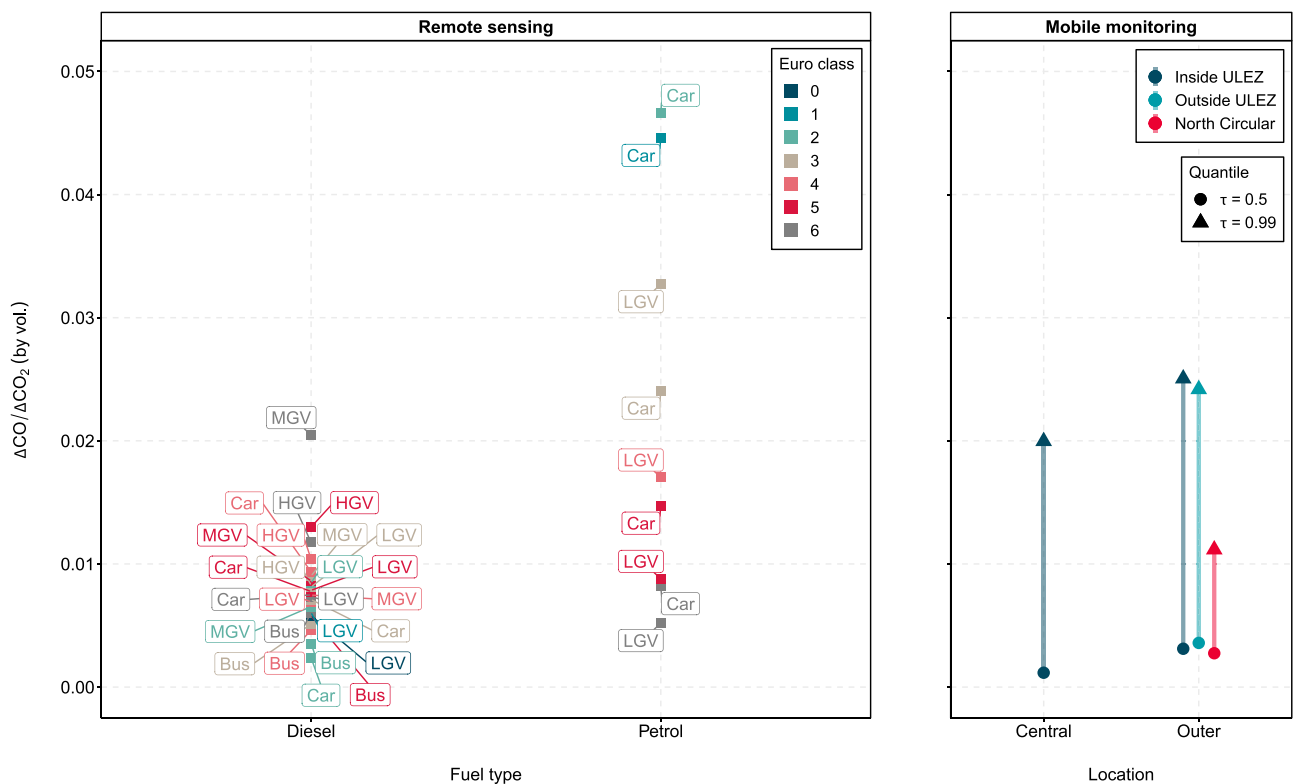


**Fig. 4.** Comparison between emission ratios of a)  $\Delta NO_x / \Delta CO_2$  and b)  $\Delta CO / \Delta CO_2$  derived from remote sensing and mobile monitoring, Left: Mean emission ratios for each vehicle category, split by vehicle type, fuel type and European emissions standard from the remote sensing observations. Right: Mean ratio derived from mobile monitoring in Central and Outer London for  $\tau = 0.5$  (circle) and  $\tau = 0.99$  (triangle). The Outer London route was further split into three sections: inside ULEZ, outside ULEZ and the North Circular road.

Euro 6/VI diesel range. As a result, the fleet-average emission intensity in Central London is doubled relative to Outer London.

Regarding Outer London, the mean  $\Delta\text{NO}_x/\Delta\text{CO}_2$  ratio was lower than Central London, whilst the opposite was true for the  $\Delta\text{CO}/\Delta\text{CO}_2$  ratio. This finding is consistent with the differences in fleet composition, where there is a larger proportion of passenger cars in Outer London, (77% compared to 60% in Central London) but a lower proportion of buses (2% compared to 10% in Central London) (Fig. S14). Consequently, it is expected that there will be a higher proportion of petrol vehicles which typically emit more CO but less  $\text{NO}_x$  than diesel, as shown in Fig. 4. There was little difference in the range of both the  $\Delta\text{NO}_x/\Delta\text{CO}_2$  ratio and  $\Delta\text{CO}/\Delta\text{CO}_2$  ratios from  $\tau = 0.5$  to  $\tau = 0.99$  between sections of the route inside and out of the ULEZ. This is consistent with the assumption that roads that lie outside of the ULEZ benefit from the policy because many trips that pass through the ULEZ either originate or terminate outside the zone (Padilla et al., 2022; Ma et al., 2021)).

A key feature of the Outer London route was the North Circular Road, a major highway which dissects the route from north to south and marks the boundary of the ULEZ. Fig. 4 shows there was a much smaller range in both the  $\Delta\text{NO}_x/\Delta\text{CO}_2$  and  $\Delta\text{CO}/\Delta\text{CO}_2$  ratios in comparison to the remainder of the Outer London route and Central London. In particular, there was a distinct lack of high-emission events responsible for elevating the 99th percentile of the emissions intensity on other parts of the road network. Evidence from Central London discussed previously suggests the highest  $\text{NO}_x$  emissions are linked to buses. The traffic count data revealed there was an almost negligible proportion of buses along the North Circular (0.2% of the fleet), which could explain the lack of such events.

Also of note was the higher proportion of HGVs on the North Circular, which made up 8% of the total counts, compared to less than 2% along the remainder of the route. On average, HGVs typically have higher  $\text{NO}_x$  emission factors than lighter vehicles such as passenger cars such that in the 2020 National Atmospheric Emissions Inventory the  $\text{NO}_x$  emission factor for rigid HGVs was  $1.43 \text{ g km}^{-1}$ , compared to  $0.52 \text{ g km}^{-1}$  for diesel cars and  $0.065 \text{ g km}^{-1}$  for petrol cars. Moreover, modern HGVs are fitted with SCR after-treatment systems to comply with the emission regulations, which emit more  $\text{NO}_x$  during urban driving but the catalysts are more effective at reducing  $\text{NO}_x$  during motorway driving at high speeds (Gao et al., 2021). Therefore, as evidenced in Central London, it might be expected that a relatively high proportion of diesel vehicles fitted with after-treatment systems would increase the  $\text{NO}_x$  emissions intensity. However, in contrast to Central London, the North Circular typically consisted of free-flowing traffic with an average speed of  $65 \text{ km h}^{-1}$ , conditions where the technology is expected to perform well. Therefore, diesel vehicles on the North Circular were not susceptible to the excess  $\text{NO}_x$  emissions seen in Central London, providing further evidence of a congestion penalty arising from the coupling of diesel vehicles in heavy traffic.

### 3.4. Conclusions and implications

Whilst it is clear that the implementation of the ULEZ has improved air quality in London, evident from the reduction in ambient concentrations of  $\text{NO}_2$  (Ma et al., 2021; Greater London Authority, 2022), our analysis suggests that the full benefits of such a scheme have not yet been realised owing to the influence of congestion. Our results imply that fleet-average  $\text{NO}_x$  emissions are doubled in Central London as a consequence of the congestion penalty, subsequently leading to a 1.6-fold increase in ambient  $\text{NO}_x$  mixing ratios. Whilst the measurement strategy in this study was designed to capture highly congested conditions, many other cities also suffer from vehicular congestion. The current work emphasises the need to consider policies such as low emission zones together with congestion mitigation strategies if optimal emissions reduction is to be achieved. It is also clear that a more detailed consideration should be given to the operation of urban buses, including the efficacy of bus retrofits in reducing emissions of  $\text{NO}_x$  and  $\text{NO}_2$ .

The regression framework described in the current work increases the number of ways in which mobile measurements can be analyzed and understood. We outline a singular methodology that offers insights into the spatial patterns of persistent emission sources, while simultaneously revealing the attributes of the most significant emitters within the vehicle fleet. This approach provides policy makers with a powerful tool, which enables the targeted development of transport interventions which are either aimed at reducing emissions in specific areas or designed to target a high-emitting subset of the fleet. Furthermore, these approaches provide a way in which to track and quantify emissions changes over time.

By validating the ambient emission ratios obtained from mobile monitoring alongside extensive remote sensing data, the mobile measurements led us to infer the presence of under-performing emission control technologies caused by congestion. Such insights are not attainable through remote sensing alone, as it is limited by the narrower range of sampling conditions required for valid measurements. Therefore, we extend the scope of insights obtained from mobile monitoring, which can also be applied to locations where remote sensing measurements are unavailable. Future applications could be related to isolating and quantifying the influence of different factors that affect emissions intensity and absolute concentrations. For example, if the measured ratios were correlated with traffic metrics such as those provided by Waze<sup>TM</sup>, inferences could be made about traffic-related pollution sources in locations with Waze<sup>TM</sup> in the absence of mobile monitoring.

### CRedit authorship contribution statement

**Shona E. Wilde:** Conceptualization, Methodology, Validation, Formal analysis, Investigation, Data curation, Visualization, Writing – original draft, Writing – review & editing. **Lauren E. Padilla:** Conceptualization, Methodology, Project administration, Supervision, Writing – review & editing. **Naomi J. Farren:** Methodology, Investigation, Writing – review & editing. **Ramón A. Alvarez:** Methodology, Project administration, Funding acquisition, Supervision, Writing – review & editing. **Samuel Wilson:** Methodology, Investigation, Writing – review & editing. **James D. Lee:** Methodology, Investigation, Writing – review & editing. **Rebecca L. Wagner:** Methodology, Investigation, Writing – review & editing. **Greg Slater:** Methodology, Writing – review & editing. **Daniel Peters:** Methodology, Writing – review & editing. **David C. Carslaw:** Conceptualization, Methodology, Investigation, Project administration, Funding acquisition, Supervision, Writing – original draft, Writing – review & editing.

### Declaration of competing interest

The authors declare that they have no known competing financial interests or personal relationships that could have appeared to influence the work reported in this paper.

### Data availability

Data will be made available on request.

### Acknowledgements

We acknowledge funding from Environmental Defense Fund, whose work is supported by gifts from Signe Ostby, Scott Cook, Valhalla Foundation, and VoLo Foundation. The authors thank Alkesh Solanki, Danny Vickers and Elizabeth Fonseca for help arranging and coordinating the logistics of the mobile monitoring platform. The authors acknowledge help from Katie Read at the University of York regarding instrument calibration and maintenance. Rebecca Wagner was supported by the NERC Panorama Doctoral Training Partnership (grant no. NE/S007458/1).

## Appendix A. Supplementary data

Supplementary data to this article can be found online at <https://doi.org/10.1016/j.aeoa.2024.100241>.

## References

- Apte, J.S., Messier, K.P., Gani, S., Brauer, M., Kirchstetter, T.W., Lunden, M.M., Marshall, J.D., Portier, C.J., Vermeulen, R.C.H., Hamburg, S.P., 2017. High-resolution air pollution mapping with google street view cars: Exploiting big data. *Environ. Sci. Technol.* 51, 6999–7008. <https://doi.org/10.1021/acs.est.7b00891>.
- Barratt, B., Carslaw, D., 2014. Impacts of the bus retrofit programme on no<sub>2</sub> concentrations along putney high street. *Environ. Res. Group, Rep. Prep, London brgh. Wandsworth*.
- Berghmans, P., Bleux, N., Panis, L.I., Mishra, V., Torfs, R., Van Poppel, M., 2009. Exposure assessment of a cyclist to pm<sub>10</sub> and ultrafine particles. *Sci. Total Environ.* 407, 1286–1298. URL: <https://www.sciencedirect.com/science/article/pii/S004896970801067X>.
- Bishop, G.A., Stedman, D.H., 2008. A decade of on-road emissions measurements. *Environ. Sci. Technol.* 42, 1651–1656.
- Bishop, G.A., Stedman, D.H., Ashbaugh, L., 1996. Motor vehicle emissions variability. *J. Air Waste Manag. Assoc.* 46, 667–675. <https://doi.org/10.1080/10473289.1996.10467501>.
- Bishop, Gary A., Brent, G., Schuchmann, D.H.S., Lawson, D.R., 2012. Multispecies remote sensing measurements of vehicle emissions on sherman way in van nuys, California. *J. Air Waste Manag. Assoc.* 62, 1127–1133. <https://doi.org/10.1080/10962247.2012.699015>.
- Böhm, M., Nanni, M., Pappalardo, L., 2022. Gross polluters and vehicle emissions reduction. *Nat. Sustain.* 5, 699–707.
- Boogaard, H., Borgman, F., Kamminga, J., Hoek, G., 2009. Exposure to ultrafine and fine particles and noise during cycling and driving in 11 Dutch cities. *Atmos. Environ.* 43, 4234–4242. <https://doi.org/10.1016/j.atmosenv.2009.05.035>.
- Buchinsky, M., 1998. Recent advances in quantile regression models: a practical guideline for empirical research. *J. Hum. Resour.* 88–126.
- Burgard, D.A., Bishop, G.A., Stadtmuller, R.S., Dalton, T.R., Stedman, D.H., 2006. Spectroscopy applied to on-road mobile source emissions. *Appl. Spectrosc.* 60, 135A–148A. <https://doi.org/10.1366/00037020677412185>.
- Carslaw, D.C., Rhys-Tyler, G., 2013. New insights from comprehensive on-road measurements of nox, no<sub>2</sub> and nh<sub>3</sub> from vehicle emission remote sensing in london, UK. *Atmos. Environ.* 81, 339–347. <https://doi.org/10.1016/j.atmosenv.2013.09.026>.
- Carslaw, D.C., Priestman, M., Williams, M.L., Stewart, G.B., Beevers, S.D., 2015. Performance of optimised scr retrofit buses under urban driving and controlled conditions. *Atmos. Environ.* 105, 70–77. <https://doi.org/10.1016/j.atmosenv.2015.01.044>.
- Chambliss, S.E., Preble, C.V., Caubel, J.J., Cados, T., Messier, K.P., Alvarez, R.A., LaFranchi, B., Lunden, M., Marshall, J.D., Szpiro, A.A., Kirchstetter, T.W., Apte, J.S., 2020. Comparison of mobile and fixed-site black carbon measurements for high-resolution urban pollution mapping. *Environ. Sci. Technol.* 54, 7848–7857. <https://doi.org/10.1021/acs.est.0c01409>.
- Chen, Y., Gu, P., Schulte, N., Zhou, X., Mara, S., Croes, B.E., Herner, J.D., Vijayan, A., 2022. A new mobile monitoring approach to characterize community-scale air pollution patterns and identify local high pollution zones. *Atmos. Environ.* 272, 118936. <https://doi.org/10.1016/j.atmosenv.2022.118936>.
- Clapp, L.J., Jenkin, M.E., 2001. Analysis of the relationship between ambient levels of O<sub>3</sub>, NO<sub>2</sub> and no as a function of NO<sub>x</sub> in the UK. *Atmos. Environ.* 35, 6391–6405. [https://doi.org/10.1016/S1352-2310\(01\)000378-8](https://doi.org/10.1016/S1352-2310(01)000378-8).
- Collet, S., Kidokoro, T., Kinugasa, Y., Karamchandani, P., DenBleyker, A., 2015. High emitter light duty vehicle contributions to on-road mobile emissions in 2018 and 2030. *Stud. Eng. Technol.* 2. <https://doi.org/10.11114/set.v2i1.838>.
- Cummings, L.E., Stewart, J.D., Reist, R., Shakya, K.M., Kremer, P., 2021. Mobile monitoring of air pollution reveals spatial and temporal variation in an urban landscape. *Front. Built Environ.* 7. <https://www.frontiersin.org/article/10.3389/fbuil.2021.648620>, 10.3389/fbuil.2021.648620.
- Davison, J., Rose, R.A., Farren, N.J., Wagner, R.L., Murrells, T.P., Carslaw, D.C., 2021. Verification of a national emission inventory and influence of on-road vehicle manufacturer-level emissions. *Environ. Sci. Technol.* 55, 4452–4461. <https://doi.org/10.1021/acs.est.0c08363>.
- Department for Environment Food & Rural Affairs, 2022. Emissions of air pollutants in the UK – nitrogen oxides. URL: <https://www.gov.uk/government/statistics/emission-s-of-air-pollutants>. (Accessed 7 July 2022).
- Department for Transport, 2021. Road traffic statistics. URL: <https://roadtraffic.dft.gov.uk/downloads>.
- Department for Transport, 2022. Vehicle licensing statistics data tables. URL: <https://www.gov.uk/government/statistical-data-sets/vehicle-licensing-statistics-data-tables>.
- Farren, N.J., Davison, J., Rose, R.A., Wagner, R.L., Carslaw, D.C., 2020. Underestimated ammonia emissions from road vehicles. *Environ. Sci. Technol.* 54, 15689–15697. <https://doi.org/10.1021/acs.est.0c05839>.
- Font, A., Guiseppin, L., Blangiardo, M., Ghersi, V., Fuller, G.W., 2019. A tale of two cities: is air pollution improving in paris and london? *Environ. Pollut.* 249, 1–12. <https://doi.org/10.1016/j.envpol.2019.01.040>.
- Gao, J., Chen, H., Liu, Y., Li, Y., Li, T., Tu, R., Liang, B., Ma, C., 2021. The effect of after-treatment techniques on the correlations between driving behaviours and no<sub>x</sub> emissions of passenger cars. *J. Clean. Prod.* 288, 125647. <https://doi.org/10.1016/j.jclepro.2020.125647>.
- Gerbig, C., Schmitgen, S., Kley, D., Volz-Thomas, A., Dewey, K., Haaks, D., 1999. An improved fast-response vacuum-uv resonance fluorescence co instrument. *J. Geophys. Res. Atmos.* 104, 1699–1704. <https://doi.org/10.1029/1998JD100031>.
- Gilman, J.B., Lerner, B.M., Kuster, W.C., de Gouw, J.A., 2013. Source signature of volatile organic compounds from oil and natural gas operations in northeastern Colorado. *Environ. Sci. Technol.* 47, 1297–1305. <https://doi.org/10.1021/es304119a>, 10.1021/es304119a.
- Grange, S.K., Farren, N.J., Vaughan, A.R., Rose, R.A., Carslaw, D.C., 2019. Strong temperature dependence for light-duty diesel vehicle nox emissions. *Environ. Sci. Technol.* 53, 6587–6596. <https://doi.org/10.1021/acs.est.9b01024>, 10.1021/acs.est.9b01024.
- Grange, S.K., Farren, N.J., Vaughan, A.R., Davison, J., Carslaw, D.C., 2020. Post-dieselgate: evidence of nox emission reductions using on-road remote sensing. *Environ. Sci. Technol. Lett.* 7, 382–387. <https://doi.org/10.1021/acs.estlett.0c00188>, 10.1021/acs.estlett.0c00188.
- Greater London Authority, 2022. Expanded ultra low emission zone six month report URL: <https://www.london.gov.uk/programmes-and-strategies/environment-and-climate-change/environment-publications/expanded-ultra-low-emission-zone-six-month-report>.
- Greater London Authority, 2023. Inner london ulez expansion 1 year report. URL: <https://www.london.gov.uk/programmes-strategies/environment-and-climate-change/environment-and-climate-change-publications/inner-london-ultra-low-emission-zone-expansion-one-year-report>.
- Hankey, S., Marshall, J.D., 2015. Land use regression models of on-road particulate air pollution (particle number, black carbon, pm<sub>2.5</sub>, particle size) using mobile monitoring. *Environ. Sci. Technol.* 49, 9194–9202. <https://doi.org/10.1021/acs.est.5b01209>, 10.1021/acs.est.5b01209. pMID: 26134458.
- Horbanski, M., Pöhler, D., Lampel, J., Platt, U., 2019. The icad (iterative cavity-enhanced doas) method. *Atmos. Meas. Tech.* 12, 3365–3381. URL: <https://amt.copernicus.org/articles/12/3365/2019/>, 10.5194/amt-12-3365-2019.
- Hu, S., Paulson, S.E., Fruin, S., Kozawa, K., Mara, S., Winer, A.M., 2012. Observation of elevated air pollutant concentrations in a residential neighborhood of los angeles California using a mobile platform. *Atmos. Environ.* 51, 311–319. <https://doi.org/10.1016/j.atmosenv.2011.12.055>.
- Hudda, N., Fruin, S., Delfino, R.J., Sioutas, C., 2013. Efficient determination of vehicle emission factors by fuel use category using on-road measurements: downward trends on los angeles freight corridor i-710. *Atmos. Chem. Phys.* 13, 347–357. URL: <https://acp.copernicus.org/articles/13/347/2013/>, 10.5194/acp-13-347-2013.
- Larson, T., Gould, T., Riley, E.A., Austin, E., Fintzi, J., Sheppard, L., Yost, M., Simpson, C., 2017. Ambient air quality measurements from a continuously moving mobile platform: estimation of area-wide, fuel-based, mobile source emission factors using absolute principal component scores. *Atmos. Environ.* 152, 201–211. <https://doi.org/10.1016/j.atmosenv.2016.12.037>.
- Li, J., Chang, H., Ma, L., Hao, J., Yang, R.T., 2011. Low-temperature selective catalytic reduction of nox with nh<sub>3</sub> over metal oxide and zeolite catalysts—a review. *Catal. Today* 175, 147–156. URL: <https://www.sciencedirect.com/science/article/pii/S0920586111002434>, 10.1016/j.cattod.2011.03.034. the 6th International Conference on Environmental Catalysis (6th ICEC) Beijing, China, September 12-15, 2010.
- Li, H.Z., Gu, P., Ye, Q., Zimmerman, N., Robinson, E.S., Subramanian, R., Apte, J.S., Robinson, A.L., Presto, A.A., 2019. Spatially dense air pollutant sampling: implications of spatial variability on the representativeness of stationary air pollutant monitors. *Atmos. Environ.* X 2, 100012. <https://doi.org/10.1016/j.aeoa.2019.100012>.
- Lozhkina, O.V., Lozhkin, V.N., 2016. Estimation of nitrogen oxides emissions from petrol and diesel passenger cars by means of on-board monitoring: effect of vehicle speed, vehicle technology, engine type on emission rates. *Transport. Res. Transport Environ.* 47, 251–264. <https://doi.org/10.1016/j.trd.2016.06.008>.
- Ma, L., Graham, D.J., Stettler, M.E.J., 2021. Has the ultra low emission zone in london improved air quality? *Environ. Res. Lett.* 16, 124001. <https://doi.org/10.1088/1748-9326/ac30c1>, 10.1088/1748-9326/ac30c1.
- Miller, D.J., Actkinson, B., Padilla, L., Griffin, R.J., Moore, K., Lewis, P.G.T., Gardner-Frolic, R., Craft, E., Portier, C.J., Hamburg, S.P., Alvarez, R.A., 2020. Characterizing elevated urban air pollutant spatial patterns with mobile monitoring in houston, Texas. *Environ. Sci. Technol.* 54, 2133–2142. <https://doi.org/10.1021/acs.est.9b05523>, 10.1021/acs.est.9b05523.
- Office of Air Quality Planning and Standards, 2017. National Emissions Inventory (NEI) 2014. U.S. Environmental Protection Agency, Research Triangle Park, N.C. URL: <https://www.epa.gov/air-emissions-inventories/2014-national-emission-inventory-nei-report>.
- Olin, M., Oikarinen, H., Marjanen, P., Mikkonen, S., Karjalainen, P., 0. High Particle Number Emissions Determined with Robust Regression Plume Analysis (Rrpa) from Hundreds of Vehicle Chases. *Environmental Science & Technology* 0, null. doi: 10.1021/acs.est.2c08198. pMID: 37282503.
- Organization, W.H., 2021. WHO Global Air Quality Guidelines: Particulate Matter (PM<sub>2.5</sub> and PM<sub>10</sub>), Ozone, Nitrogen Dioxide, Sulfur Dioxide and Carbon Monoxide. *World Health Organization*.
- Padilla, L.E., Ma, G.Q., Peters, D., Dupuy-Todd, M., Forsyth, E., Stidworthy, A., Mills, J., Bell, S., Hayward, I., Coppin, G., Moore, K., Fonseca, E., Popoola, O.A., Douglas, F., Slater, G., Tuxen-Bettman, K., Carruthers, D., Martin, N.A., Jones, R.L., Alvarez, R.A., 2022. New methods to derive street-scale spatial patterns of air pollution from mobile monitoring. *Atmos. Environ.* 270, 118851. <https://doi.org/10.1016/j.atmosenv.2021.118851>.

- R Core Team, 2022. R: A Language and Environment for Statistical Computing. R Foundation for Statistical Computing, Vienna, Austria. URL: <https://www.R-project.org/>.
- Richards, P., Terry, B., Chadderton, J., Vincent, M.W., 2004. Retrofitting urban buses to reduce pm and no. SAE Trans. 113, 1129–1138. URL: <http://www.jstor.org/stable/44740833>.
- Salmon, O.E., Shepson, P.B., Ren, X., He, H., Hall, D.L., Dickerson, R.R., Stirn, B.H., Brown, S.S., Fibiger, D.L., McDuffie, E.E., Campos, T.L., Gurney, K.R., Thornton, J. A., 2018. Top-down estimates of nox and co emissions from Washington, d.c.-baltimore during the winter campaign. J. Geophys. Res. Atmos. 123, 7705–7724. <https://doi.org/10.1029/2018JD028539>.
- Shoari, N., Heydari, S., Blangiardo, M., 2022. School neighbourhood and compliance with who-recommended annual no2 guideline: a case study of greater london. Sci. Total Environ. 803, 150038 <https://doi.org/10.1016/j.scitotenv.2021.150038>.
- Smit, R., Bainbridge, S., Kennedy, D., Kingston, P., 2021. A decade of measuring on-road vehicle emissions with remote sensing in Australia. Atmos. Environ. 252, 118317. URL: <https://www.sciencedirect.com/science/article/pii/S1352231021001357>. doi:10.1016/j.atmosenv.2021.118317.
- Sun, K., Tao, L., Miller, D.J., Pan, D., Golston, L.M., Zondlo, M.A., Griffin, R.J., Wallace, H.W., Leong, Y.J., Yang, M.M., Zhang, Y., Mauzerall, D.L., Zhu, T., 2017. Vehicle emissions as an important urban ammonia source in the United States and China. Environ. Sci. Technol. 51, 2472–2481. <https://doi.org/10.1021/acs.est.6b02805>.
- Tan, Y., Lipsky, E.M., Saleh, R., Robinson, A.L., Presto, A.A., 2014. Characterizing the spatial variation of air pollutants and the contributions of high emitting vehicles in pittsburgh. Environ. Sci. Technol. 48, 14186–14194. <https://doi.org/10.1021/es5034074>.
- The International Council on Clean Transportation, 2017. The Impact of Improved Regulation of Real-World NO<sub>x</sub> Emissions from Diesel Passenger Cars in the Eu, pp. 2015–2030.
- TomTom Traffic Index, 2023. London is the world's slowest city: a closer look at the data. URL: <https://www.tomtom.com/newsroom/explainers-and-insights/london-is-the-worlds-slowest-city/>.
- Wagner, R.L., Farren, N.J., Davison, J., Young, S., Hopkins, J.R., Lewis, A.C., Carslaw, D. C., Shaw, M.D., 2021. Application of a mobile laboratory using a selected-ion flow-tube mass spectrometer (sift-ms) for characterisation of volatile organic compounds and atmospheric trace gases. Atmos. Meas. Tech. 14, 6083–6100. <https://amt.copernicus.org/articles/14/6083/2021/>, 10.5194/amt-14-6083-2021.
- Watson, A.Y., Bates, R.R., Kennedy, D., 1988. Atmospheric transport and dispersion of air pollutants associated with vehicular emissions. In: Air Pollution, the Automobile, and Public Health. National Academies Press (US).
- Wen, Y., Wang, H., Larson, T., Kelp, M., Zhang, S., Wu, Y., Marshall, J.D., 2019. On-highway vehicle emission factors, and spatial patterns, based on mobile monitoring and absolute principal component score. Sci. Total Environ. 676, 242–251. <https://doi.org/10.1016/j.scitotenv.2019.04.185>.
- Wilde, S., 2021. Mobilemeasr: Tools to Perform Data Analysis on Mobile Measurements. R package version 0.1.0.
- Wilde, S.E., Dominutti, P.A., Allen, G., Andrews, S.J., Bateson, P., Bauguitte, S.J.B., Burton, R.R., Colfescu, I., France, J., Hopkins, J.R., Huang, L., Jones, A.E., Lachlan-Cope, T., Lee, J.D., Lewis, A.C., Mobbs, S.D., Weiss, A., Young, S., Purvis, R.M., 2021. Speciation of voc emissions related to offshore north sea oil and gas production. Atmos. Chem. Phys. 21, 3741–3762. <https://acp.copernicus.org/articles/21/3741/2021/>, 10.5194/acp-21-3741-2021.
- Xu, H., Luo, Z., Wang, N., Qu, Z., Chen, J., An, L., 2019. Experimental study of the selective catalytic reduction after-treatment for the exhaust emission of a diesel engine. Appl. Therm. Eng. 147, 198–204. <https://doi.org/10.1016/j.applthermaleng.2018.10.067>. URL: <https://www.sciencedirect.com/science/article/pii/S1359431118336937>.
- Yacovitch, T.I., Herndon, S.C., Roscioli, J.R., Floerchinger, C., McGovern, R.M., Agnese, M., Pétron, G., Kofler, J., Sweeney, C., Karion, A., Conley, S.A., Kort, E.A., Nöhle, L., Fischer, M., Hildebrandt, L., Koeth, J., McManus, J.B., Nelson, D.D., Zahniser, M.S., Kolb, C.E., 2014. Demonstration of an ethane spectrometer for methane source identification. Environ. Sci. Technol. 48, 8028–8034. <https://doi.org/10.1021/es501475q>, 10.1021/es501475q.
- Yang, L., Franco, V., Campestrini, A., German, J., Mock, P., 2015. Nox Control Technologies for Euro 6 Diesel Passenger Cars: Market Penetration and Experimental Performance Assessment.
- Zavala, M., Herndon, S.C., Slott, R.S., Dunlea, E.J., Marr, L.C., Shorter, J.H., Zahniser, M., Knighton, W.B., Rogers, T.M., Kolb, C.E., Molina, L.T., Molina, M.J., 2006. Characterization of on-road vehicle emissions in the mexico city metropolitan area using a mobile laboratory in chase and fleet average measurement modes during the mcma-2003 field campaign. Atmos. Chem. Phys. 6, 5129–5142. <https://acp.copernicus.org/articles/6/5129/2006/>, 10.5194/acp-6-5129-2006.
- Zavala, M., Herndon, S.C., Wood, E.C., Jayne, J.T., Nelson, D.D., Trimborn, A.M., Dunlea, E., Knighton, W.B., Mendoza, A., Allen, D.T., Kolb, C.E., Molina, M.J., Molina, L.T., 2009. Comparison of emissions from on-road sources using a mobile laboratory under various driving and operational sampling modes. Atmos. Chem. Phys. 9, 1–14. URL: <https://acp.copernicus.org/articles/9/1/2009/>, 10.5194/acp-9-1-2009.
- Zhou, L., Hallquist, Å.M., Hallquist, M., Salvador, C.M., Gaita, S.M., Sjödin, Å., Jerksjö, M., Salberg, H., Wängberg, I., Mellqvist, J., Liu, Q., Lee, B.P., Chan, C.K., 2020. A transition of atmospheric emissions of particles and gases from on-road heavy-duty trucks. Atmos. Chem. Phys. 20, 1701–1722. URL: <https://acp.copernicus.org/articles/20/1701/2020/>, 10.5194/acp-20-1701-2020.
- Zhu, Y., Chen, J., Bi, X., Kuhlmann, G., Chan, K.L., Dietrich, F., Brunner, D., Ye, S., Wenig, M., 2020. Spatial and temporal representativeness of point measurements for nitrogen dioxide pollution levels in cities. Atmos. Chem. Phys. 20, 13241–13251. URL: <https://acp.copernicus.org/articles/20/13241/2020/>, 10.5194/acp-20-13241-2020.